Translational Science

Cancer Research

Selective mTORC2 Inhibitor Therapeutically Blocks Breast Cancer Cell Growth and Survival

Thomas A. Werfel[1,2], Shan Wang[3], Meredith A. Jackson[1], Taylor E. Kavanaugh[1], Meghan Morrison Joly[2], Linus H. Lee[1], Donna J. Hicks[2], Violeta Sanchez[4], Paula Gonzalez Ericsson[4], Kameron V. Kilchrist[1], Somtochukwu C. Dimobi[1], Samantha M. Sarett[1], Dana M. Brantley-Sieders[3,4], Rebecca S. Cook[1,2,4], and Craig L. Duvall[1]

Abstract

Small-molecule inhibitors of the mTORC2 kinase (torkinibs) have shown efficacy in early clinical trials. However, the torkinibs under study also inhibit the other mTOR-containing complex mTORC1. While mTORC1/mTORC2 combined inhibition may be beneficial in cancer cells, recent reports describe compensatory cell survival upon mTORC1 inhibition due to loss of negative feedback on PI3K, increased autophagy, and increased macropinocytosis. Genetic models suggest that selective mTORC2 inhibition would be effective in breast cancers, but the lack of selective small-molecule inhibitors of mTORC2 have precluded testing of this hypothesis to date. Here we report the engineering of a nanoparticle-based RNAi therapeutic that can effectively silence the mTORC2 obligate cofactor Rictor. Nanoparticle-based Rictor ablation in HER2-amplified breast tumors was achieved following intratumoral and intravenous delivery, decreasing Akt phosphorylation and increasing tumor cell killing. Selective mTORC2 inhibition *in vivo*, combined with the HER2 inhibitor lapatinib, decreased the growth of HER2-amplified breast cancers to a greater extent than either agent alone, suggesting that mTORC2 promotes lapatinib resistance, but is overcome by mTORC2 inhibition. Importantly, selective mTORC2 inhibition was effective in a triple-negative breast cancer (TNBC) model, decreasing Akt phosphorylation and tumor growth, consistent with our findings that RICTOR mRNA correlates with worse outcome in patients with basal-like TNBC. Together, our results offer preclinical validation of a novel RNAi delivery platform for therapeutic gene ablation in breast cancer, and they show that mTORC2-selective targeting is feasible and efficacious in this disease setting.

Significance: This study describes a nanomedicine to effectively inhibit the growth regulatory kinase mTORC2 in a preclinical model of breast cancer, targeting an important pathogenic enzyme in that setting that has been undruggable to date. *Cancer Res; 78(7); 1845–58. ©2018 AACR.*

Introduction

Approximately 20% of breast cancers overexpress HER2, which activates the PI3K/Akt/mTOR signaling cascade that drives tumor cell growth, survival, metabolism, and motility (1). Targeting HER2 therapeutically using trastuzumab or tyrosine kinase inhibitors (TKIs; e.g., lapatinib, neratinib) inhibits PI3K/Akt/mTOR signaling and decreases growth and survival of $HER2^+$ breast cancers. The development of anti-HER2 therapeutics has significantly improved clinical outcomes for patients with $HER2^+$ breast cancers (2). However, resurgent PI3K/Akt/mTOR signaling allows tumors to evade cell death in response to HER2 inhibition, is associated with tumor recurrence, and is a major cause of therapeutic resistance for anti-HER2 treatment strategies. Moreover, PI3K/Akt/mTOR signaling is aberrantly elevated in up to 60% of clinical breast cancers across all subtypes [$HER2^+$, ER^+, PR^+, and triple-negative breast cancer (TNBC)], due to genetic alterations in *PIK3CA*, *AKT1-3*, *PTEN*, and increased expression or activity of growth factors and their receptors (3, 4). Given its prevalent activation in breast cancers and prominent role downstream of HER2, there is significant motivation to pursue new treatment strategies targeting the PI3K/Akt/mTOR signaling axis.

The intracellular serine/threonine kinase mTOR exists in two structurally and functionally distinct complexes that lie downstream of HER2 and PI3K (5). The protein Rictor, in association with mTOR, is a defining and required cofactor of mTOR complex 2 (mTORC2), while the protein Raptor is a required cofactor for mTOR complex 1 (mTORC1), although the two complexes affiliate with other common (e.g., mLST8) and distinct (e.g., PRAS40; Sin1) protein cofactors that support complex stability, negative regulation, and substrate affinity. The two complexes are differentially inhibited by rapamycin and rapamycin-related drugs called rapalogs; mTORC1 is extremely sensitive, but mTORC2 is insensitive to this drug class, although in some cell types an extended treatment with rapamycin can impair mTORC2 signaling (6). These two complexes are functionally disparate as well. Signaling through mTORC1 is responsive to intracellular levels of

[1]Department of Biomedical Engineering, Vanderbilt University, Nashville, Tennessee. [2]Department of Cell and Developmental Biology, Vanderbilt University School of Medicine, Nashville, Tennessee. [3]Department of Medicine, Vanderbilt University Medical Center, Nashville, Tennessee. [4]Breast Cancer Research Program, Vanderbilt-Ingram Cancer Center, Vanderbilt University Medical Center, Nashville, Tennessee.

Note: Supplementary data for this article are available at Cancer Research Online (http://cancerres.aacrjournals.org/).

Corresponding Authors: Craig L. Duvall, Department of Biomedical Engineering, Vanderbilt University School of Engineering, Nashville, TN 37232. Phone: 615-322-3598; Fax: 615-343-7919; E-mail: craig.duvall@vanderbilt.edu; and Rebecca S. Cook, Phone: 615-936-3813; E-mail: rebecca.cook@vanderbilt.edu

doi: 10.1158/0008-5472.CAN-17-2388

oxygen, amino acids, and ATP, among others, activates anabolic cellular metabolism (e.g., DNA synthesis, protein translation), and inhibits biological processes associated with nutrient deprivation (e.g., autophagy, macropinocytosis; ref. 7). Interestingly, mTORC1 signaling also dampens PI3K signaling via a negative feedback cycle involving IRS-1 (8–10).

In contrast, mTORC2 phosphorylates AGC kinases (Akt, SGK, and PKC family members; refs. 11–16), each with known oncogenic roles in tumor cell survival (12, 15, 17–22) and cytoskeletal dynamics that drive planar cell motility, a key step in metastasis (23). Genetic Rictor ablation has been previously used to eliminate mTORC2 signaling and block Akt S473 phosphorylation (a direct mTORC2 phosphorylation site). Rictor ablation from the mammary epithelium of genetically engineered mice revealed a role for mTORC2 in motility and invasion of the normal mammary epithelium during branching morphogenesis (15). This phenotype was carried forward to mouse models of spontaneous breast cancer, revealing that loss of Rictor-dependent mTORC2 activity decreased tumor cell survival in an Akt-dependent manner (24) and blocked metastasis in a manner depending on an Akt, Tiam-1, and Rac1-dependent signaling cascade (25). Findings related to the therapeutic potential of mTORC2 as a target in genetically engineered mouse models are supported by a growing body of literature showing that genetic mTORC2 inhibition (using Rictor RNAi) also reduces cell motility and survival in cultured human breast cancer cell lines (24, 26–28). Further strengthening the clinical implications, immunohistochemical (IHC) analyses revealed higher Rictor staining in clinical invasive breast carcinomas (IBC) over normal breast epithelium, and showed that Rictor IHC staining intensity correlated with higher grade (grade II/III) tumors (24). In support of this finding, we discovered that *RICTOR* gene copy number gains are associated with decreased overall survival in patients with IBC (24).

Preclinical and clinical genetic studies support targeted inhibition of mTORC2 for improving breast cancer patient outcomes, and several studies suggest that inhibition of mTORC2 while sparing mTORC1 signaling is desirable (7–10). The lack of availability of an mTORC2-selective inhibitor has previously limited the ability to rigorously test the value of selective mTORC2 inhibition as a therapeutic approach for treating established tumors. Unfortunately, potent and selective small-molecule mTORC2 inhibitors that spare mTORC1 activity are very difficult to generate due to the intricate, multifaceted protein–protein interactions of the mTORC2 complex. On the basis of an abundance of evidence demonstrating that genetic Rictor ablation impairs mTORC2 signaling while sparing mTORC1 signaling, we sought to develop a Rictor-specific RNAi nanomedicine that enables therapeutic inhibition of mTORC2 activity. This approach leverages nanoparticles optimized for intravenous (i.v.) delivery of siRNA to tumors (29) that here, for the first time, are applied against a therapeutically relevant gene target, Rictor, that is otherwise selectively undruggable. A potent Rictor RNAi formulation was developed, confirmed to be mTORC2-selective, and verified to provide *in vivo* efficacy in both HER2-amplified and TNBCs. Furthermore, in the setting of HER2-amplified disease, Rictor-targeted therapy was found to cooperate with the HER2 kinase inhibitor lapatinib to regress existing tumors. While other studies have provided insights on Rictor deletion inhibiting HER2-amplified tumor development (24), herein the first evidence is provided on the therapeutic benefit of an mTORC2-selective inhibitor in existing tumors, and the therapeutic promise of mTORC2-selective inhibition against TNBCs is shown.

Materials and Methods

Materials

All chemicals were purchased from Sigma-Aldrich unless otherwise specified. DMAEMA and BMA monomers were passed twice through an activated basic alumina gravity column prior to use to remove inhibitors. 2,2-Azobis(2-methylpropionitrile) (AIBN) was recrystallized twice from methanol. All cell culture reagents were purchased through Thermo Fisher Scientific unless otherwise specified. Cell culture media and reagents, including DMEM, fetal bovine serum, phosphate buffered saline (PBS) containing or lacking $Ca2^{+}$ and $Mg2^{+}$ (+/+ and −/−, respectively), and Antibiotic-Antimycotic Reagent were purchased through Life Technologies. For dynamic light scattering experiments, dsDNA was used as a model for siRNA. For all fluorescent measurements, fluorophore-labeled dsDNA was used a model of siRNA. A list of oligonucleotides is provided in the Supplementary Fig. S1. *RICTOR* siRNAs were acquired from Dharmacon's human ON-TARGETplus siRNA library (set of 4: ON-TARGETplus RICTOR siRNA; LQ-016984-00-0002). Additional *RICTOR* siRNAs were acquired from IDT's human DsiRNA library (hs.Ri.RICTOR.13.1, hs.Ri.RICTOR.13.2, hs.Ri.RICTOR.13.3, hs.Ri.RICTOR.13.4, hs.Ri.RICTOR.13.5). The naming scheme used for ternary siRNA-loaded nanoparticle (si-NP) formulation is as follows: [Binary Polymer] (Binary N:P)-[Ternary Polymer](Ternary N:P). Therefore, ternary si-NPs containing a DB core formulated at 4:1 N:P and PDB corona formulated to a final N:P of 12:1 are referred to as DB4-PDB12.

Polymer synthesis and si-NP generation

Polymers and si-NPs were synthesized and characterized according to previously published chemical procedures (29). Supplementary Figures S2–S5 describe the synthesis scheme and validate the composition of all polymers and si-NPs used within these studies.

Cell line authentication

BT474, MDA-MB-361, SKBR3, and MDA-MB-231 cells were purchased in 2012 from ATCC and cultured at low passage in DMEM with 10% FCS and 1% Antibiotic-Antimycotic Reagent (Gibco). Cell identity was verified by ATCC using genotyping with a Multiplex STR assay. All cell lines were screened monthly for mycoplasma using the procedure of Young and colleagues (30). All cell lines were used for experiments within 50 passages from thawing.

Cell culture

Human breast cancer cells were seeded (MDA-MB-231: 50,000 cells per well; MDA-MB-361, SKBR3, BT474: 250,000 cells per well) in 6-well plates and transfected with Lipofectamine 2000 (LF2K) carrying either scrambled or Rictor siRNA (20 nmol/L) shown in Supplementary Fig. S1. Where indicated, cells were treated with lapatinib (Selleck Chem) dissolved in dimethyl sulfoxide (DMSO). Cell growth in monolayer was assessed using a crystal violet assay as described previously (24). Luciferase-expressing MDA-MB-231 cells were described previously (31). YFP-G8 MDA-MB-231 cells were generated by transduction with VSV-G pseudotyped Moloney murine leukemia virus (MMLV)

retroviral particles encoding yellow fluorescent protein-(YFP-) Galectin 8 and blasticidin resistance (32). For si-NP experiments, cells were seeded (MDA-MB-231: 50,000 cells per well; MDA-MB-361, SKBR3, BT474: 250,000 cells per well) in 6-well plates, adhering overnight before adding si-NPs (100 nmol/L siRNA) for 24 hours, then replenished with fresh media.

Reverse transcription and qRT-PCR

RNA was isolated with an RNEasy Mini Kit (Qiagen) according to the manufacturer's protocol at 48 hours. The expression of Rictor and Raptor were evaluated by qRT-PCR by normalizing to the housekeeping gene GAPDH. RNA was extracted from tumor tissue using a tissue lyser (Qiagen) and Qiazol and isolated using the RNEasy Universal Mini Kit (Qiagen) according to the manufacturer's protocol. Rictor mRNA levels were evaluated by qRT-PCR and normalized to the housekeeping gene, *36B4*.

Western blotting and immunoprecipitation

Cells or tumors were homogenized in ice-cold lysis buffer [50 mmol/L Tris pH 7.4, 100 mmol/L NaF, 400 mmol/L NaCl, 0.5% NP-40, 100 μmol/L Na_3VO_4, 1× protease inhibitor cocktail (Roche)] and cleared by centrifugation (4°C, 13,000 × *g*, 10 minutes). Protein concentration was determined using BCA assay (Pierce), then samples were resolved by SDS-PAGE. For immunoprecipitation, 1 mg total protein in 1 mL of low salt lysis buffer [50 mmol/L Tris pH 7.4, 100 mmol/L NaF, 120 mmol/L NaCl, 0.5% NP-40, 100 μmol/L Na_3VO_4, 1× protease inhibitor cocktail (Roche)] was immunoprecipitated with anti-mTOR antibody (Cell Signaling Technology) or a normal IgG control using Protein A/G+ beads (Santa Cruz Biotechnology), washed 5 times with low salt lysis buffer, and then denatured in 4× reducing sample buffer (Novex). Proteins separated by SDS-PAGE were transferred to nitrocellulose membranes. Membranes were blocked and probed with antibodies as described previously (33) using primary antibodies: α-actin (Sigma-Aldrich); Rictor (Santa Cruz Biotechnology); and the following from Cell Signaling Technology [phospho-cocktail; AKT, P-Akt S473, S6, P-S6, and Raptor].

Caspase-3/7 activity

MDA-MB-361, BT474, SKBR3, and MDA-MB-231 cells (5,000 cells per well) were seeded in black-walled 96-well plates and allowed to adhere overnight. After treatment, half of the media was removed (leaving 50 μL behind). To the remaining media and adherent cells, 50 μL of Caspase 3/7 Glo reagent (Promega) was added. After 1-hour incubation on a shaker at room temperature, luminescence was measured on an IVIS Lumina III imaging system (Xenogen Corporation).

Colony formation assays, mTORC2 inhibitor, and lapatinib therapy

MDA-MB-361, SKBR3, and BT474 cells (5,000 cells per well) were seeded in 6-well plates on day 0. Cells were treated with si-NPs carrying either scrambled or Rictor siRNA (100 nmol/L each) on day 1. Cells were fed with fresh media containing 0.25 μmol/L lapatinib in DMSO, or with an equal volume of DMSO (0.2 μL) every 3 days through day 10. Cells were stained with crystal violet on day 10, and scanned on a flatbed scanner.

Human breast cancer dataset analysis

Overall survival of patients with Rictor and HER2 alterations >2 SD from mean of expression was analyzed within The Cancer Genome Atlas METABRIC dataset. All 2,509 samples from the METABRIC dataset were included and mutations, copy number alterations, and mRNA expression >2 SD from the mean were included as alterations.

Mice

For generation of orthotopic breast cancer xenografts, 1×10^6 tumor cells were injected into the inguinal mammary fatpads of athymic Balb/C *nu/nu* female mice (4–6 weeks old, Jax Mice). Tumor dimensions were measured using digital calipers. Tumor volume was calculated as: volume = length × width^2 × 0.52; ref. 34). For bioluminescence imaging, tumor-bearing mice were injected intraperitoneally (i.p.) with luciferin substrate (150 mg/kg) and imaged on IVIS Lumina III (Xenogen Corporation) 30 minutes postinjection. For intratumoral si-NP delivery, 1 mg/kg (siRNA dose) si-NPs were delivered in 50 μL volume of saline to anesthetized mice. For intravenous si-NP delivery, 1 mg/kg (siRNA dose) si-NPs were delivered in 100 μL volume of saline via tail vein injection. Fluorescence imaging of tissues following intravenous si-NP delivery was performed with IVIS Lumina III imaging system (Xenogen Corporation) at excitation wavelength of 620 ± 5 nm and emission wavelength of 670 ± 5 nm. Where shown, mice were treated with 100 mg/kg lapatinib or equal volume of vehicle control (0.1% Tween-80, 0.5% methyl cellulose) by oral gavage.

Flow cytometry

Intracellular delivery of Cy5 si-NPs was evaluated by flow cytometry. Tumors were incubated with collagenase (0.5 mg/mL, Roche Life Sciences) and DNAse (0.19 mg/mL, Bio-Rad) for 1 hour, incubated with 5 mmol/L EDTA for 20 minutes, resuspended in HBSS, and filtered through a 70-μm nylon cell strainer. Erythrocytes were removed with ACK lysis buffer (Thermo Fisher Scientific) for 2 minutes, and washed cells were assessed by flow cytometry (BD LSRii, BD Biosciences). Uptake analysis was performed in FlowJo. Cell populations were isolated using forward and side scatter, then GFP-positive tumor cells were selected, and Cy5 fluorescence intensity was measured.

Histologic analysis

Tissue processing, hematoxylin and eosin (H&E) staining, and IHC for Ki67 was performed by the Vanderbilt Translational Pathology Shared Resource. Tumors were resected from mice, and paraffin sections (5-μm) were stained with H&E (Calbiochem). IHC on paraffin-embedded sections was performed as described previously (35) using: Rictor (Santa Cruz Biotechnology), Ki67 (Santa Cruz Biotechnology) and P-Akt S473 (Cell Signaling Technology) antibodies. Immunodetection was performed using the Vectastain kit (Vector Laboratories), according to the manufacturer's directions. TUNEL staining was performed using the ApopTag In Situ Red Apoptosis Detection Kit (Millipore) per the manufacturer's protocol. Photomicrographs were acquired on an Olympus CK40 inverted microscope through an Optronics DEI-750C charge-coupled-device video camera using CellSens capture software. CellSens software was also used to quantify the average percentage of Ki67 or TUNEL-positive nuclei as described previously (36).

Ethics statement

All animals were housed under pathogen-free conditions, and experiments were performed in accordance with AAALAC

guidelines and with Vanderbilt University Institutional Animal Care and Use Committee approval.

Statistical analysis

Treatment groups were compared using either two-tailed Student *t* test or one-way ANOVA test coupled with Tukey means comparison test, where $P < 0.05$ was deemed representative of a significant difference between treatment groups. For tumor growth kinetics, linear regression of the growth curves was performed, and a significant difference is indicated where the 95% confidence intervals of curves do not overlap. Outliers were removed from data using the Grubb method with $\alpha = 0.05$ for a single outlier or ROUT method with a 1% Q-value for multiple outliers. For all data, the arithmetic mean and SE are shown.

Results

Screening Rictor siRNA sequences for nanoparticle-mediated delivery to *HER2*-amplified and TNBC cell cultures

Recently published work described an optimized si-NP, comprised of three components: (i) siRNA, (2) core-forming polymer (poly(DMAEMA-*co*-BMA), DB_4), and (iii) PEGylated, corona-forming polymer (PEG-*b*-poly(DMAEMA-*co*-BMA), PDB_{12}; Fig. 1A; Supplementary Figs. S2–S5; ref. 29). We employed these optimized ternary si-NPs to deliver Rictor-targeting siRNA sequences to cells *in vitro* and tumors *in vivo*. Consistent with previously published reports, particle assembly with siRNA and core-forming polymer (but lacking the corona polymer) generated large, unstable structures (Supplementary Fig. S6A), while particle assembly with core-forming and corona-forming polymers (but lacking the siRNA) generated very small micelles (~20 nm diameter) (Supplementary Fig. S6A). However, the ternary particle harboring all three components produced stable si-NPs with uniform size (~150 nm diameter; Supplementary Fig. S6A and S6B), and with no evidence of binary pre-NPs (DB_4 + siRNA). These ternary si-NPs loaded with nontargeting siRNA sequences (100 nmol/L final concentration) were delivered to the cultured media of MDA-MB-361, BT474, SKBR3, and MDA-MB-231 breast cancer cells without any other additive or transfection reagent. This si-NP formulation was well tolerated by all cell lines tested, with 70%–90% cell viability (Supplementary Fig. S6C). The si-NPs displayed potent and controlled pH-dependent membrane disruption beginning at pH 6.8 and below (Supplementary Fig. S6D), consistent with the pH of endolysosomal compartments and confirming optimization for endolysosomal escape, a critical attribute for siRNA intracellular cytosolic bioavailability and therapeutic potency (29, 31, 37). Endosome disruption was confirmed using a novel approach, in which galectin 8 (G8), a protein rapidly recruited to damaged endosomes, is fused with yellow fluorescent protein (YFP). YFP-G8 recruitment to damaged endolysosomes, visualized by fluorescent puncta can be used as a surrogate pharmacodynamic marker for endosomal escape (32, 38). We found that MDA-MB-231 TNBC cells treated with ternary si-NPs displayed >7-fold increase in fluorescent YFP-G8 puncta at disrupted endosomes over what was seen in cells prior to treatment (Supplementary Fig. S6E), supporting the utility of the ternary si-NPs for siRNA delivery to cells.

A panel of nine *RICTOR* siRNA sequences was transiently transfected with Lipofectamine into MDA-MB-361 cells, a *HER2*-amplified breast cancer cell line previously shown to express high *RICTOR* levels, screening for the sequence providing the greatest *RICTOR* knockdown. qRT-PCR analysis revealed nearly 70% decreased *RICTOR* transcript levels in cells transfected with sequence siRic.2 (Fig. 1B), which was used for all further studies. Importantly, a scrambled siRNA sequence was used as a negative control, which did not provide significant alteration in relative *RICTOR* transcript levels as compared with untreated cells (NT). Transient transfection of the Rictor siRNA siRic.2 into *HER2*-amplified breast cancer cell lines MDA-MB-361, BT474, and SKBR3 resulted in >70% knockdown of *RICTOR* transcripts (Fig. 1C). To confirm that the selected Rictor siRNA sequence resulted in selective mTORC2 inhibition as described in previous work from our laboratory and others, we assessed phosphorylation of mTORC2 and mTORC1 effectors, Akt and ribosomal protein S6, respectively (Fig. 1D). Western blot analysis confirmed Rictor was decreased in *HER2*-amplified MDA-MB-361 cells and MDA-MB-231 cells (a human TNBC cell line) at 24 hours after transfection with siRictor (Fig. 1E). Akt phosphorylation at S473 (the mTORC2 phosphorylation site) was diminished in MDA-MB-361 cells transfected with siRic.2 (Fig. 1E), consistent with previous results. Similar results were seen in MDA-MB-231 cells. Notably, Rictor knockdown did not decrease phosphorylation of the mTORC1 effector S6 in MDA-MB-361 or MDA-MB-231 cells, suggesting that Rictor knockdown selectively inhibits mTORC2 activity while sparing mTORC1. Conversely, Raptor knockdown using siRNA decreased Raptor protein levels, and decreased phosphorylation of the mTORC1 effector S6, but did not diminish phosphorylation of the mTORC2 effector Akt. As expected, the combination of Rictor knockdown with Raptor knockdown resulted in decreased phosphorylation to both S6 and Akt S473, suggesting inhibition of both mTORC1 and mTORC2. Association between Raptor and mTOR, a required step in mTORC1 activation, was not affected by Rictor knockdown using siRic.2 sequences, as measured by coprecipitation (Fig. 1F). Rictor coprecipitation in mTOR immunoprecipitates was diminished upon Rictor knockdown, together suggesting that siRic.2 sequences produce the expected molecular features of selective mTORC2 inhibition that has been described previously for Rictor knockdown. Together, these data support Rictor as an ideal candidate for further study in the setting of si-NP delivery to breast tumor cells. Although these studies using transfection of Rictor siRNA were largely confirmatory of the known molecular signaling pathways, these results represent the necessary groundwork for identification of potent Rictor siRNA and confirmation of on-target effect, data that enable rigorous testing of therapeutic nanoparticle-based Rictor siRNA delivery.

Nanoparticle-based mTORC2 delivery in combination with lapatinib decreases growth of *HER2*-amplified breast cancer cells

si-NPs harboring Rictor siRNA sequences (Rictor si-NPs) or scrambled siRNA sequences (scramble si-NPs) were delivered at a final concentration of 100 nmol/L siRNA to the culture media of *HER2*-amplified (MDA-MB-361, BT474, and SKBR3) and TNBC (MDA-MB-231) cells, without any transfection reagent or other additive. Treatment of cells with Rictor si-NPs for 24 hours silenced *RICTOR* mRNA levels 75%–90% (Fig. 2A) and increased caspase-3/7 activity (Fig. 2B). MDA-MB-361 cells

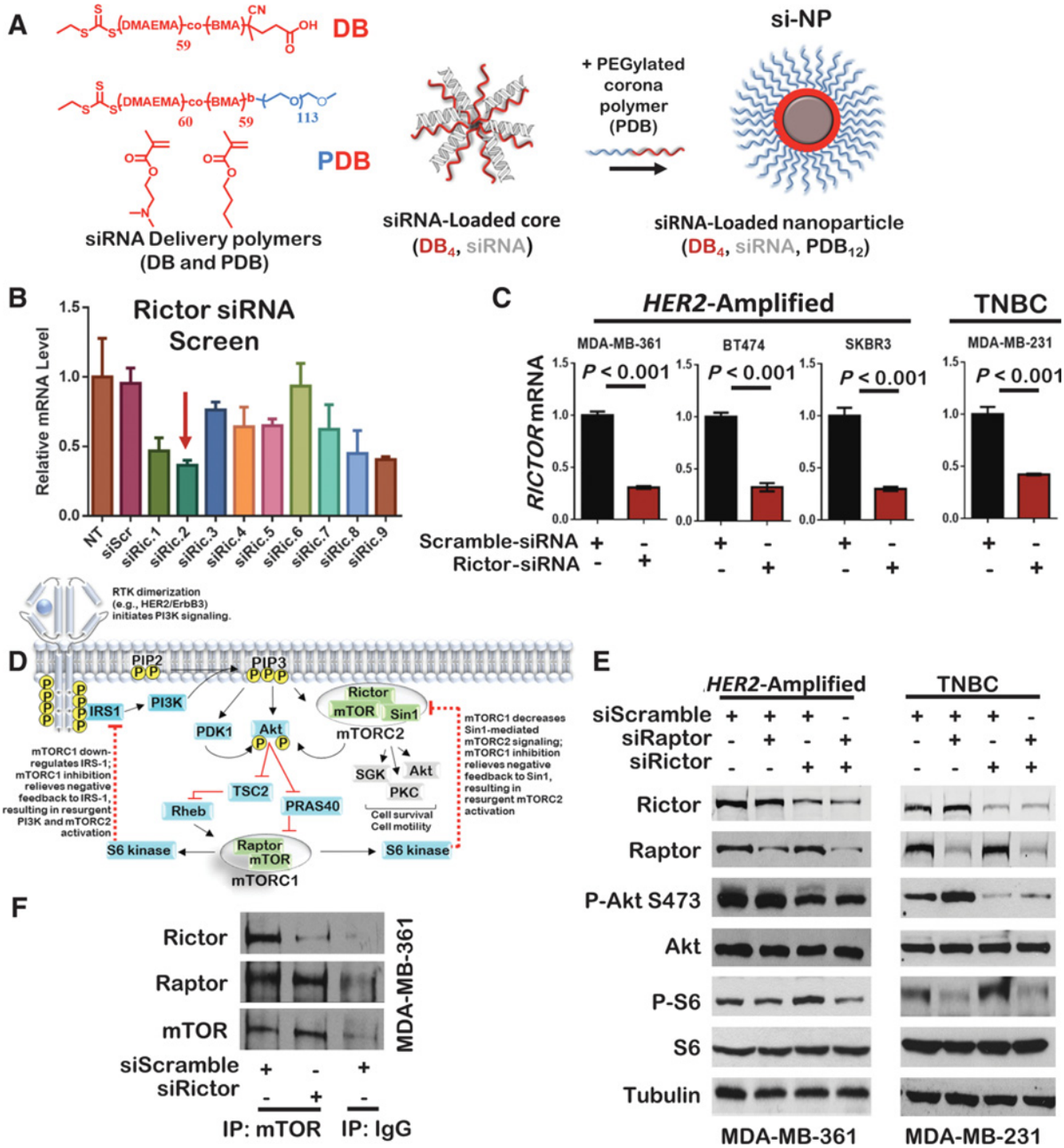

Figure 1.

RNAi selectively inhibits Rictor/mTORC2 while sparing activity of Raptor/mTORC1. **A,** Ternary si-NP nanotechnology for delivery of siRNA to tumors *in vivo*. DB polymers form an initial polymer–siRNA complex that is stabilized by the addition of a PDB polymer corona. **B,** qRT-PCR for relative *RICTOR* expression in cells 24 hours after individual siRNAs were transfected into MDA-MB-361. *RICTOR* levels in untreated cells (NT) were given a value of 1. Average ± SE is shown, $n = 3$. Arrow indicates the RICTOR siRNA sequence achieving the greatest level of knockdown and selected for further analysis. **C,** qRT-PCR for relative *RICTOR* expression in cells 24 hours after individual siRNAs were transfected into breast cancer cell lines. Relative *RICTOR* levels in cells transfected with a scrambled siRNA were given a value of 1 for each cell line. Average ± SE is shown, $n = 3$, each measured in triplicate. **D,** A schematic of key signaling effectors of mTORC2 and mTORC1 is shown. **E,** Western blot analysis of breast cancer cells transfected with siRNA sequences for Rictor and Raptor. Antibodies used are shown at the left of each panel. **F,** Western blot analysis of anti-mTOR immunoprecipitates from cells transfected with siRNA sequences against Rictor or scrambled siRNA sequences. Antibodies used for Western blot analysis are shown at the left of each panel.

treated with Rictor si-NPs for 16 hours followed by culture in normal growth media (10% serum) were assessed at 24 hours after treatment began, revealing Rictor protein knockdown through 96 hours posttreatment (Fig. 2C). Importantly, lapatinib modestly decreased, but did not completely block P-Akt S473. While P-Akt remained modestly diminished through 96

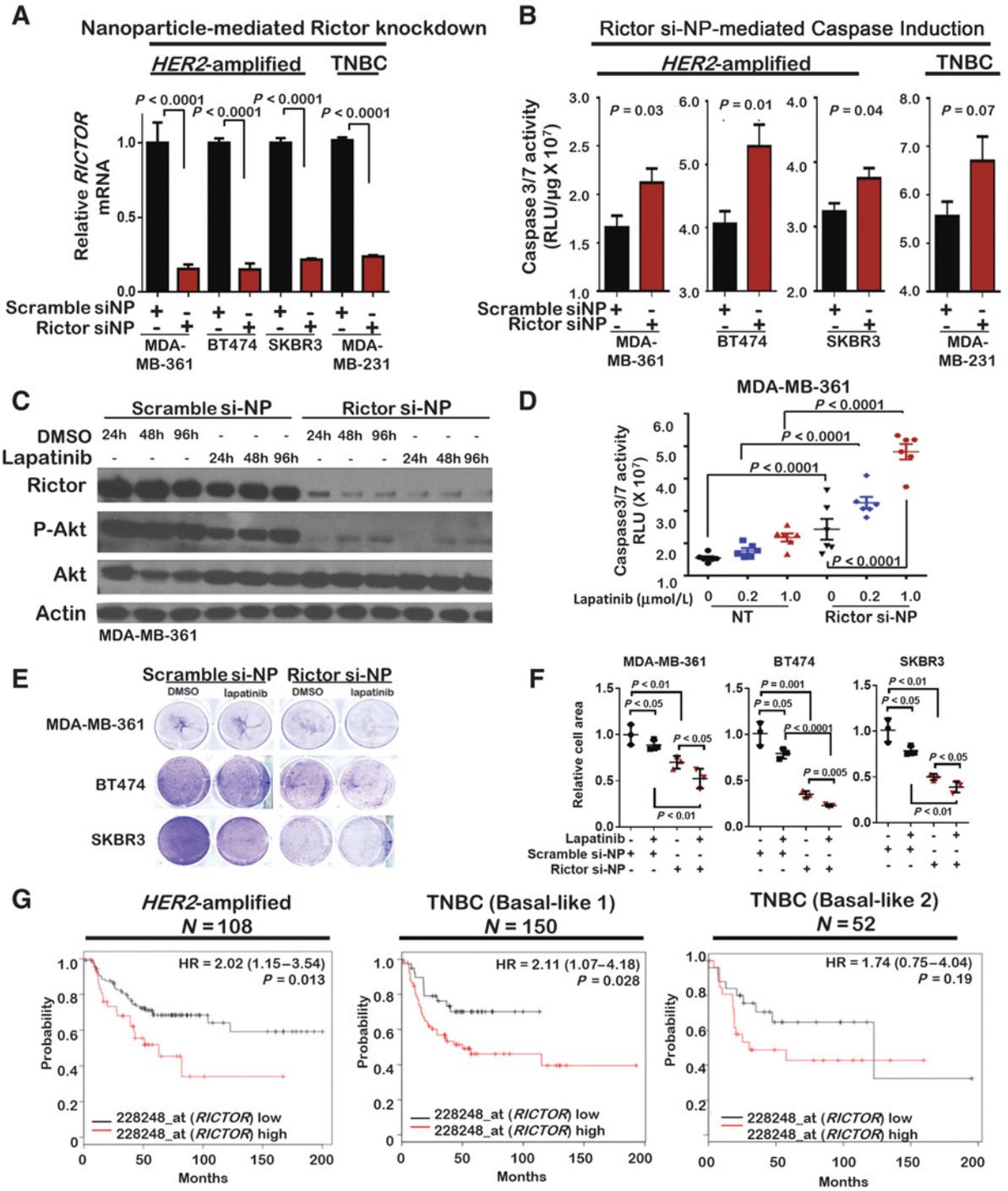

Figure 2.

si-NP-mediated Rictor knockdown blocks mTORC2 signaling and induces cell death in breast cancer cells. **A,** qRT-PCR for relative *RICTOR* expression in cells 24 hours after si-NPs were added to media. *RICTOR* levels in scramble si-NP–treated cells were given a value of 1 for each cell line. Average ± SE is shown, $n = 3$, each measured in triplicate. **B,** Caspase-3/7 activity [measured as relative light units (RLU) and corrected for total protein] was measured 24 hours after treating with si-NPs. Average ± SE, $n = 3$ (each assessed in duplicate) is shown. **C,** Western blot analysis of cells 24–96 hours after si-NP treatment ± lapatinib (1 mmol/L) or DMSO. Antibodies are indicated to the left of each panel. **D,** Caspase-3/7 activity was measured as described in **B** from cells treated 24 hours with si-NPs and lapatinib at doses shown. $N = 6$, each measured in duplicate. **E** and **F,** Cells were treated with si-NPs, then cultured with 250 nmol/L lapatinib (or DMSO) for 10 days, replacing lapatinib (but not si-NPs) every 3 days, then stained with crystal violet and imaged. **E,** Representative images. **F,** Quantitation of stained area using Image J software. The midlines are the average (±SE), $N = 3$ replicates, each assessed in duplicate. **G,** Kaplan–Meier curves showing PFS in meta-analysis of breast cancer populations selected for breast cancer subtype using KmPlot software (KmPlot.org) and separated into patients whose tumors express high *RICTOR* (probe 228248_at) versus others. Log-rank test.

hours in response to lapatinib, the P-Akt levels increased over time between 24 to 96 hours. This pattern of resurgent P-Akt following HER2 molecular targeting has been reported previously, and is thought to drive treatment resistance (2). Furthermore, mTORC2 inhibition (using stable Rictor shRNA expression) has been shown to confer increased sensitivity to the HER2 kinase inhibitor lapatinib, in large part due to improved inhibition of P-Akt (24). Therefore, we tested the combination of Rictor si-NPs with lapatinib (1 μmol/L), which decreased P-Akt to a far greater extent than lapatinib alone (Fig. 2C). Importantly, the combination of lapatinib + Rictor si-NPs increased caspase-3/7 activity >2-fold beyond what was seen with either lapatinib alone or Rictor si-NPs alone (Fig. 2D). Culture of MDA-MB-361, BT474, and SKBR3 cells for 10 days with lapatinib (250 nmol/L) revealed decreased tumor cell growth (Fig. 2E). However, treatment of cells for 24 hours with Rictor si-NPs followed by 10-day culture with lapatinib decreased tumor cell growth to an even greater extent (Fig. 2E and F). These findings support the use of Rictor si-NPs as a means of selective mTORC2 targeting in *HER2*-amplified breast cancer cells, recapitulating results previously achieved using standard technologies to deliver Rictor RNAi sequences, but without the use of transfection reagents or viral infection.

RICTOR levels correlate with worse outcome in *HER2*-amplified breast cancers and TNBC subtypes

Previous studies demonstrate that *RICTOR* gene amplification correlates with worse outcome in patients with invasive breast cancer (IBC; ref. 24). This was confirmed in analysis of METABRIC-curated invasive breast cancers ($N = 2{,}509$) assessed for *RICTOR* gene alterations, including gene amplification, mutation, or overexpression (RNA expressed > 2 SD from the mean). This assessment demonstrated significant correlation between *RICTOR* alterations and decreased overall survival (OS) for IBC patients (Supplementary Fig. S7A). The outcome was substantially worse in patients harboring *RICTOR* alterations and/or gene amplification of *ERBB2*, also known as *HER2* (Supplementary Fig. S7A). To assess more directly the impact of *RICTOR* gene expression on outcome of patients with *HER2*-amplified breast cancers, we used KmPlot software for meta-analysis of multiple breast cancer expression datasets, focusing specifically on *HER2*-amplified breast cancers ($N = 108$). This approach revealed that *HER2*-amplified breast cancers harboring high *RICTOR* mRNA levels suffered profoundly decreased progression-free survival (PFS) as compared with the remaining patients with *HER2*-amplified breast cancers in this analysis (Fig. 2G, left). This finding is consistent with previous reports demonstrating that mTORC2 activity, measured in reverse-phase protein array (RPPA) as P-Akt S473, correlates with decreased OS in patients with *HER2*-amplified breast cancer (24), and supports the use of *HER2*-amplified breast cancers as a model to test therapeutic mTORC2-selective inhibitors.

We reiterated this approach on the same collection of breast cancer expression datasets to determine whether *RICTOR* expression correlates with PFS in other breast cancer molecular subtypes. We assessed *RICTOR* levels in five subtypes of TNBC [Basal-like 1 (BL1), Basal-like 2 (BL2), immunomodulatory (IM), luminal androgen receptor (LAR), and mesenchymal (M); ref. 39], revealing a significant correlation between high *RICTOR* levels and decreased PFS in BL1 tumors ($N = 150$; Fig. 2G, middle). A similar trend was observed between high *RICTOR* levels and decreased PFS in patients with BL2 ($N = 52$; Fig. 2G, right), although this trend was not seen in other TNBC subtypes (Supplementary Fig. S7B), These findings highlight the distinct molecular phenotypes of each TNBC subtype, and suggest that some TNBC subtypes might benefit from mTORC2 inhibition.

Intratumoral delivery of si-NPs to block mTORC2 signaling blocks Akt and impairs tumor cell survival

Prior to intravenous testing of Rictor si-NPs, we confirmed that si-NP delivery to tumors was capable of target gene ablation. Toward this goal, we treated luciferase-expressing MDA-MB-231 tumors with si-NPs loaded with siRNA sequences directed against luciferase (Luc si-NP) as described previously (37). For these initial experiments, we used intratumoral delivery of Luc si-NPs and scramble si-NPs to orthtopically grown MDA-MB-231 xenografts in each of the contralateral inguinal mammary fatpads. This approach allowed target gene knockdown to be monitored in paired tumors in a longitudinal manner. At the time of treatment (0 hour), tumor bioluminescence was similar in samples treated with scramble si-NPs and contralateral tumors treated with Luc si-NPs (Fig. 3A). However, at 24 hours, bioluminescence was abolished in tumors treated with Luc si-NPs, but remained high in tumors treated with scramble si-NPs, consistent with previous observations using this model system, and supporting continued investigations using this delivery platform for intratumoral Rictor knockdown.

Because the effect of therapeutic Rictor ablation in TNBCs is unknown, we next assessed the impact of Rictor si-NPs on MDA-MB-231 tumors. Intratumoral delivery of si-NPs (1 mg/kg) began when tumors were between 50 and 100 mm^3, occurring on treatment days 0, 2, and 4 (Fig. 3B). Tumors harvested on day 5 (24 hours after final tumor treatment) revealed substantial Rictor knockdown in tumors treated with Rictor si-NPs, as measured by Western blot analysis (Fig. 3C) and IHC (Fig. 3D). Similar to what was found in MDA-MB-231 tumors, intratumoral delivery of Rictor si-NPs to orthotopic MDA-MB-361 tumors (*HER2*-amplified) also resulted in decreased Rictor protein expression (Fig. 3D). IHC further revealed that Akt phosphorylation at S473 was substantially diminished in MDA-MB-231 and MDA-MB-361 tumors treated with Rictor si-NPs, confirming deactivation of mTORC2 in these tumors. Tumor volume measurements at days 1, 3, and 5 (24 hours after each treatment) revealed that Rictor si-NPs blocked growth of MDA-MB-231 tumors and MDA-MB-361 tumors throughout the treatment period, as compared with tumors treated with scramble si-NPs, which increased tumor volume >3-fold over this time period (Fig. 3E). Reduced tumor volume was due, at least in part, to increased tumor cell death, as measured by terminal dUTP nick end labeling (TUNEL) analysis (Fig. 3F), demonstrating >8-fold induction of tumor cell death upon intratumoral Rictor knockdown in MDA-MB-231 and MDA-MB-361 tumors.

Intravenous delivery of si-NPs supports tumor gene targeting

Therapeutic feasibility of Rictor si-NPs will require systemic delivery for most tumor types, including breast cancers. Importantly, previously published studies using this ternary si-NP platform has demonstrated reduced clearance from kidneys

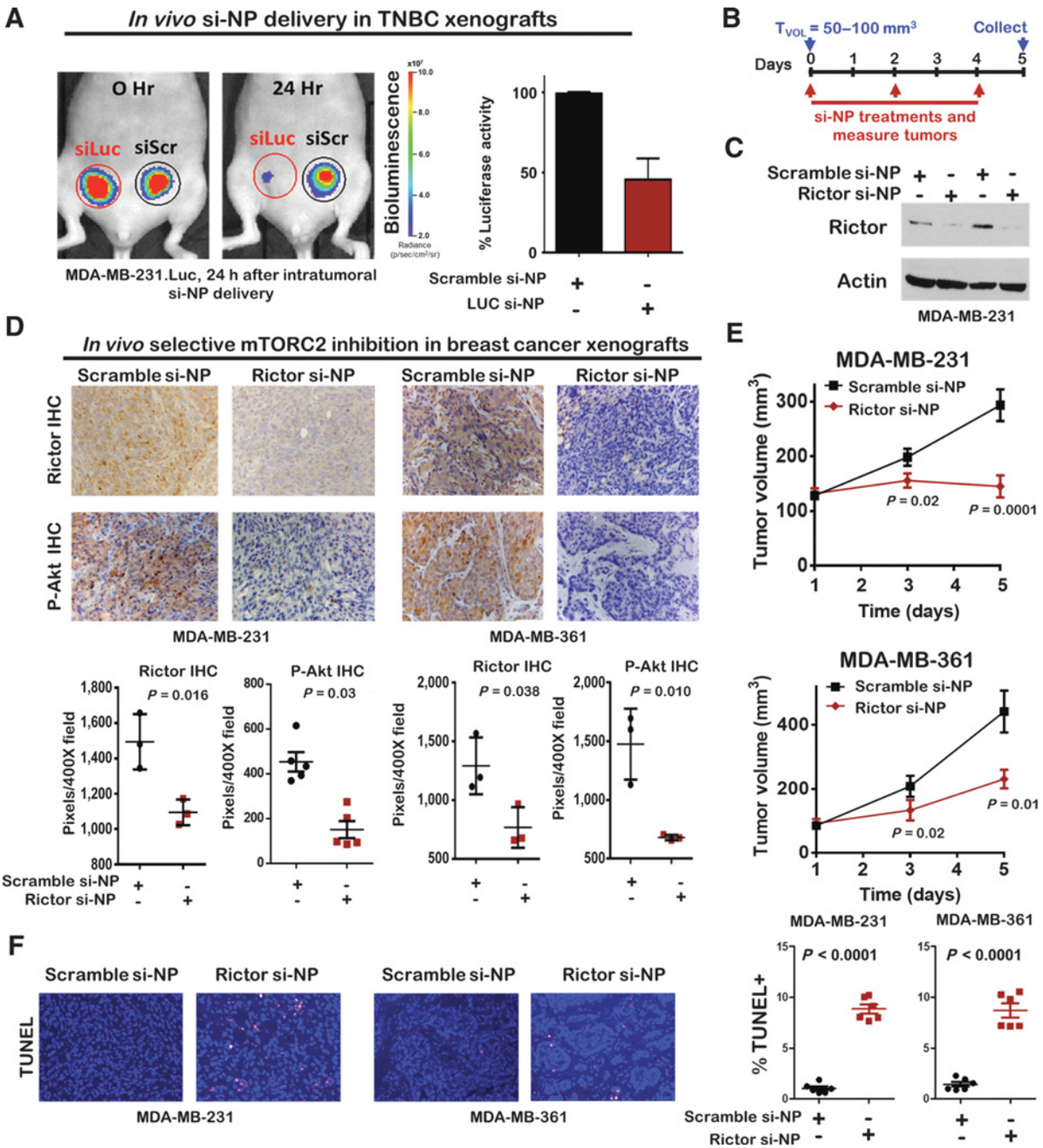

Figure 3.

Intratumoral delivery of nanoparticles provides therapeutic mTORC2 inhibition *in vivo*. **A,** MDA-MB-231-Luciferase xenografts grown in contralateral mammary fat pads were treated by intratumoral injection with luciferase si-NPs (siLuc) or scramble si-NPs (siScr). Intravital imaging of tumor luminescence was measured 24 hours after treatment with si-NPs using IVIS. Left, representative images of a single mouse imaged at 0 hours and again at 24 hours after intratumoral si-NP delivery. Right, luciferase activity at 24 hours posttreatment, as a percentage of values measured at 0 hours. Average values (±SE) shown, $n = 3$. **B,** Timeline schematic illustrates the dosing schedule for MDA-MB-231 and MDA-MB-361 tumors treated with si-NPs. Three doses were given at 48-hour intervals. Tumors were measured immediately prior to dosing. **C,** Western blot analysis of whole tumor extracts harvested on day 5, 24 hours after the final si-NP treatment. Each lane represents a tumor collected from different mice. Antibodies are shown at left of each panel. **D,** Rictor and P-Akt S473 were detected by IHC in tumors harvested on treatment day 5. Top, representative images taken at 20×. Bottom, quantitative analysis of staining using Scion Image software, expressed as pixels/field. Each point represents the average of five randomly chosen fields per sample. Midlines are the average (± SE). $n = 3$ (Rictor IHC) and 5 (P-Akt S473 IHC). **E,** Tumor volumes were measured on treatment days 0, 2, and 4, $n = 5$, average ± SE. **F,** TUNEL analysis. Left, representative images. Right, quantitation of TUNEL staining, expressed as the percentage of nuclei that are TUNEL+ $n = 6$, each assessed in five randomly chosen 40× fields.

and favorable circulation time as compared with prototypes of the technology (37). To assess si-NP distribution after intravenous delivery, we began by using si-NPs assembled with fluorescently labeled nontargeting siRNA sequences and treated tumor-bearing mice to confirm that si-NPs deliver the siRNA cargo to tumors. Tumors (MDA-MB-231), kidneys, liver, spleen, heart, and lungs were harvested 24 hours after tail vein injection of si-NPs (1 mg/kg siRNA). Nearly 20% of the total fluorescent signal was detected within tumor tissue (Fig. 4A and B). While siRNA fluorescence was similar in tumors and kidneys, little fluorescence was measured in liver, lungs, and heart. Importantly, ternary si-NPs exhibited 1.6-fold more signal within tumors as compared with the liver, although fluorescent signal in kidneys remained greater than what was seen in tumors. High signal within the kidneys is expected within this class of polyion complex si-NPs due to interruption of electrostatic interactions by heparan sulfates of the kidney glomerular basement membrane (40). However, this si-NP formulation was previously shown to decrease accumulation in kidneys to half of what was seen with other polyion–siRNA complexes (29). Furthermore, significant accumulation is not expected to occur in the kidneys; rather, this signal is expected to represent a benign route of excretion into the urine. To analyze the homogeneity of siRNA delivery to tumor cells, we harvested orthotopic MDA-MB-231 xenografts 24 hours after intravenous si-NP delivery, disaggregated tumors, and monitored the percent of tumor cells that were positive for uptake of the fluorescent (Cy5) nontargeting siRNA by flow cytometry. These studies revealed that with only a single treatment, nearly 80% of tumor cells from si-NP–treated mice were $Cy5^+$ (Fig. 4C), with an 8-fold increase in mean fluorescence intensity per cell as compared with what was seen in saline-treated mice (Fig. 4C and D), suggesting a robust and homogenous delivery of si-NPs to tumor cells using intravenous delivery. To confirm the bioactivity of si-NPs upon delivery to tumor cells, we tracked the bioluminescence of luciferase-expressing MDA-MB-231 tumors after delivery of either scramble si-NPs as a control or Luc si-NPs that knockdown luciferase expression. Bioluminescent imaging at 0, 24, and 48 hours revealed that a single delivery of Luc si-NPs diminished luminescent signal in tumors by approximately 50% compared with scramble si-NPs (Fig. 4E), confirming that si-NPs deliver bioactive siRNA strands to tumor cells and thus can achieve target gene knockdown after intravenous delivery.

Therapeutic mTORC2 inhibition using intravenous delivery of Rictor si-NPs blocks growth of *HER2*-amplified breast cancers *in vivo*

As a rigorous test of Rictor gene targeting *in vivo* with systemic, intravenous-delivered si-NPs, we began treating mice harboring MDA-MB-361 tumors grown orthotopically when tumors reached 50–100 mm^3. Mice were treated by intravenous delivery of Rictor si-NPs or scramble si-NPs (1 mg/kg siRNA) via tail vein injection on days 0, 2, 4, and 7 (Fig. 5A). Mice were further randomized to receive daily treatment with lapatinib (100 mg/kg daily by gavage) or vehicle. Although si-NPs treatment ceased at treatment day 7, daily treatment with lapatinib continued until tumors were harvested on treatment day 21. A small cohort of tumors was collected at treatment day 7 to assess the acute impact of each treatment arm on *RICTOR* expression, revealing that *RICTOR* expression decreased >60% in tumors from mice treated with Rictor si-NPs alone as compared with those treated with scramble si-NPs alone (Fig. 5B), correlating with substantially reduced Rictor protein expression in tumors (Fig. 5C), and confirming on-target activity of Rictor siRNA sequences in tumors following intravenous delivery. Interestingly, *RICTOR* transcripts were insignificantly reduced by approximately 25% in samples treated with lapatinib (Fig. 5B), although levels of Rictor protein assessed immunehistologically were not visibly altered by treatment with lapatinib. As expected, lapatinib in combination with either Scramble si-NPs or Rictor si-NPs robustly blocked tyrosine phosphorylation of HER2, validating that the known, on-target molecular effect of lapatanib was operative within tumors (Fig. 5C). Importantly, the combination of Rictor si-NPs + lapatinib diminished *RICTOR* mRNA levels >50% and decreased Rictor protein levels as compared with what was seen in tumors treated with scramble si-NPs + lapatinib (Fig. 5B and C). *RICTOR* levels in tumors treated with lapatinib + Rictor si-NPs were not statistically diminished as compared with what was seen in tumors treated with Rictor si-NPs alone. Consistent with previous reports that resurgent P-Akt S473 occurs after sustained treatment with lapatinib, we found that P-Akt was readily detected in samples harvested from mice treated with scramble si-NPs and either with or without lapatinib (Fig. 5C). However, P-Akt S473 was reduced in tumors from mice treated with intravenous Rictor si-NPs, both in the presence and absence of lapatinib, suggesting that Rictor si-NPs effectively blocked tumor mTORC2 signaling following intravenous delivery. Together, these data show that selective mTORC2 inhibition using Rictor si-NP blocks signaling through key HER2 pathway effectors, and when used in combination with lapatinib, can block signaling through compensatory signaling pathways that contribute to resistance to HER2 inhibitors.

As expected, daily oral treatment with lapatinib for 21 days reduced volumetric growth of MDA-MB-361 xenografts by approximately 50% (Fig. 5D). A similar level of growth inhibition through treatment day 21 was seen upon intravenous delivery of Rictor si-NPs, despite the fact that the final si-NP delivery occurred on treatment day 7. Furthermore, the combination of intravenous Rictor si-NP deliver through treatment day 7 plus daily oral lapatinib produced partial tumor regression through treatment day 7 (Fig. 5E), after which tumor volume remained stable, demonstrating superior control of tumor growth upon combined inhibition of HER2 (using lapatinib) and mTORC2 (using Rictor si-NPs; Fig. 5F). Histologic analyses confirmed decreased tumor size (Fig. 5G) and tumor cellular content (Fig. 5H) in samples treated with Rictor si-NPs as compared with those treated with scramble si-NPs. Notably, tumor size and cellular content were further diminished in samples treated with the combination of lapatinib + Rictor si-NPs (Fig. 5H and I), with a corresponding increase in acellular matrix in tumors treated with the combination of Rictor si-NP and lapatinib. The intravenous delivery of ternary si-NPs for Rictor therapy was also well-tolerated by the mice, with no change in glucose levels, no toxicity to liver and kidneys detected on the basis of serum markers, and no change in animal body mass (Supplementary Figs. S8A–S8C and S9).

Discussion

Previous studies demonstrate that Rictor gene targeting in mouse models of breast cancer, or using RNAi technologies

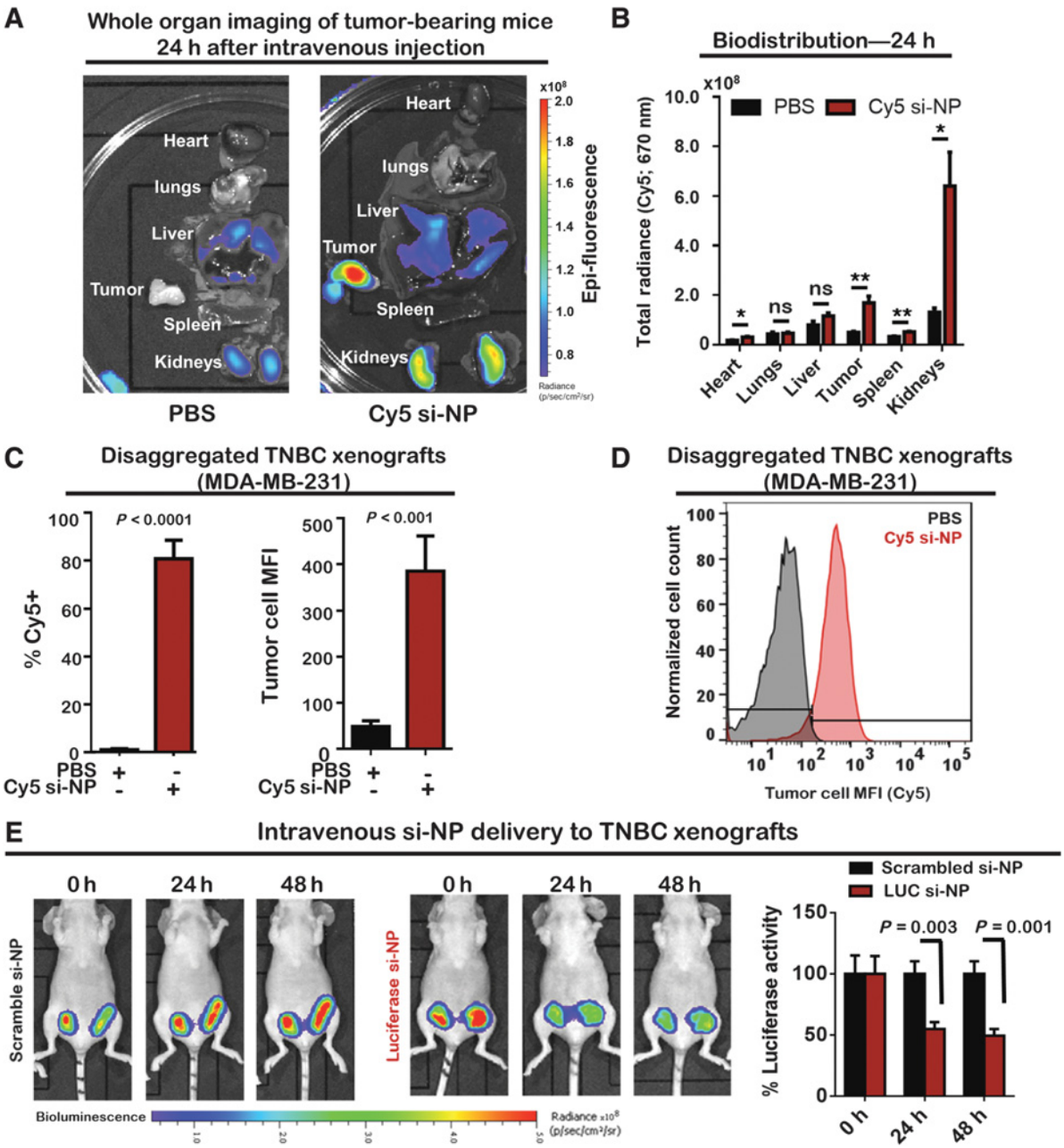

Figure 4.

Intravenous delivery of si-NPs enables tumor accumulation of siRNA and target gene knockdown *in vivo*. **A** and **B,** Whole organs and tumors (MDA-MB-231. GFP$^+$) were collected in PBS and then imaged for Cy5 fluorescence (IVIS) at 30 minutes after intravenous delivery of Cy5 si-NPs to Balb/C *nu/nu* mice. **A,** Representative images of Cy5 fluorescence are shown on the left. **B,** Quantitation of Cy5 fluorescence per organ is shown, $N = 6$. Values are the average fluorescent signal at 670 nm ($\pm$ SE). **C** and **D,** Tumors were harvested 30 minutes after intravenous si-NP delivery, disaggregated into single-cell suspensions and assessed by flow cytometry. **C,** Flow cytometric quantitation of the percentage of GFP$^+$ tumors cells harboring Cy5+ fluorescence (left) and the mean fluorescence intensity (MFI) measured for Cy5 (670 nm). Values shown are the average values of $N = 5$ experiments, $\pm$ SE. **D,** Flow cytometric detection of fluorescence in GFP$^+$ tumors cells, showing the distribution of Cy5 fluorescence throughout the tumor cell population. Representative histogram is shown. $N = 5$. **E,** LUC si-NPs or scramble si-NPs were delivered by intravenous injection to tumor-bearing mice. Vital bioluminescence of MDA-MB-2321.LUC tumors was assessed 0, 24, and 48 hours after si-NP delivery (IVIS). Representative images of intravital tumor luminescence at each time point are shown for one mouse from each group (left panels). Luminescence was quantitated at each time point. The average value measured in scramble si-NP controls was set to 100%, such that each value for each time point is expressed as a percentage of the average value measured in the controls at that same time point. $N = 5$ per group; average $\pm$ SE.

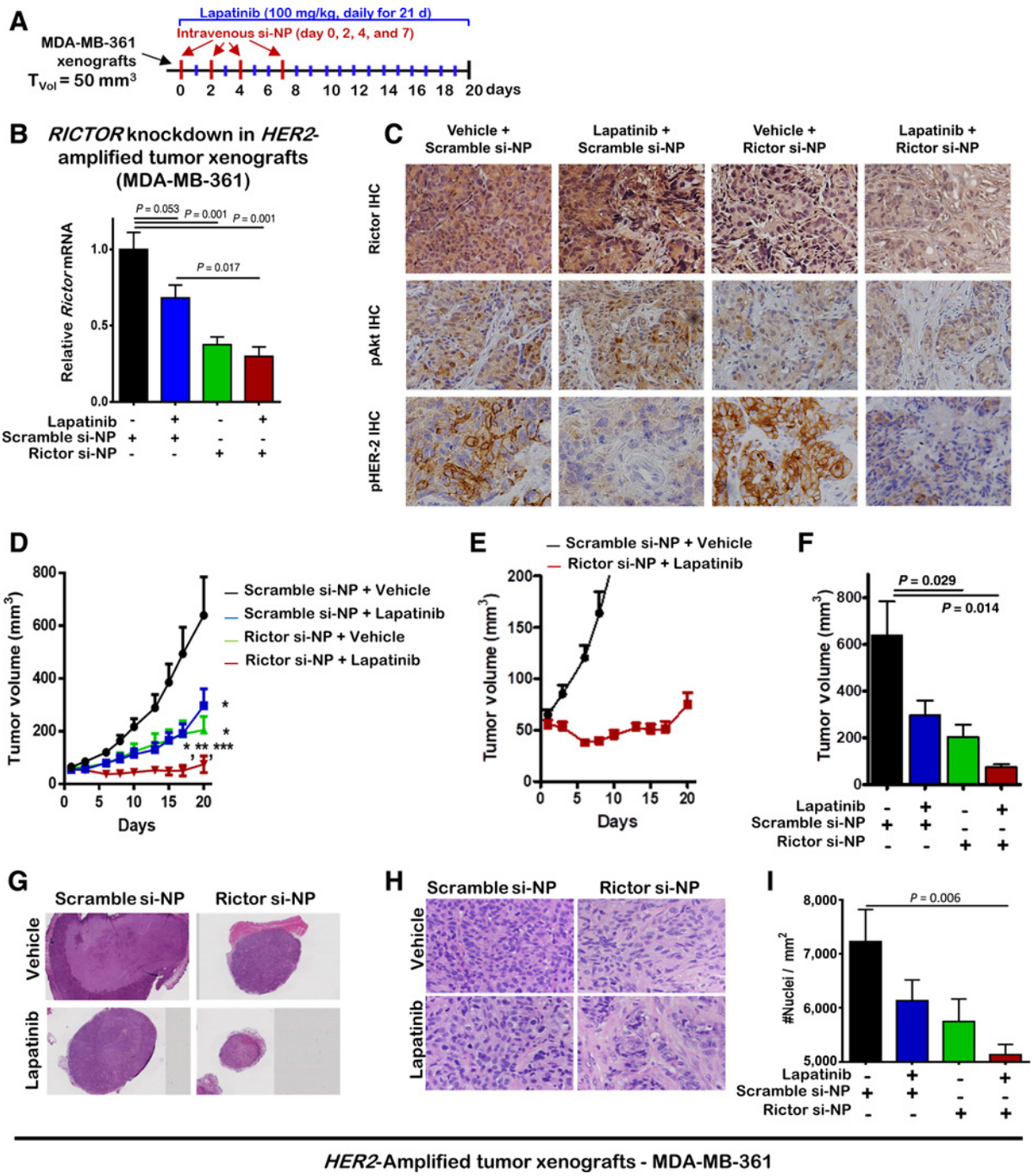

Figure 5.

Intravenous delivery of Rictor si-NPs inhibits tumor mTORC2 activity and cooperates with lapatinib to support tumor regression. **A,** MDA-MB-361 tumors grown in nude mice were treated with 1 mg/kg si-NPs (i.v. delivered on treatment days 0, 2, 4, and 7) and 100 mg/kg lapatinib (orally, once daily for 21 days). **B** and **C,** Tumors were harvested on treatment day 8, 24 hours after final si-NP treatment and 1 hour after lapatinib treatment. **B,** Whole tumor RNA was used to assess *RICTOR* gene expression levels by RT-qPCR. *RICTOR* C_t values were corrected for housekeeping gene 36B4 and are shown as the average values (± SE) relative to the average value measured in control tumors treated with vehicle and scramble si-NP. $N = 5$. **C,** IHC for Rictor, P-Akt S473, and P-HER-2. Representative images are shown. $N = 3$. **D–F,** Tumor volume was measured throughout the 21-day treatment period. Values shown are the average (± SE), $N = 7$. **G–I,** Histologic analysis of tumors collected on treatment day 21 was performed on H&E-stained sections at low power (2×, **G**) and high power (40×, **H**), demonstrating smaller size and decreased cellularity. **I,** The number of nuclei per mm^2 was determined using CellSense software. $N = 3$ randomly chosen fields per sample, $N = 5$, average ± SE.

in human breast cancer cells, eliminates mTORC2 assembly and activity. Rictor ablation by these strategies decreases signaling through key pathways including Akt, PKC, SGK, ILK, and Rac1 that regulate cell motility, cell survival, and metastasis. Enzymatic inhibition of mTOR kinase using torkinibs has proven effective at blocking mTORC2 signaling, although this occurs at the expense of mTORC1 signaling. Because mTORC1 inhibition relieves negative feedback on PI3K-to-mTORC2 signaling, torkinib-mediated inhibition of mTORC1/mTORC2 blocks tumor growth better than rapalogs (8, 9, 41–45). Superior efficacy of torkinibs in preclinical models suggests that mTORC2 inhibition provides a therapeutic benefit, albeit one that is currently unattainable without also blocking mTORC1. In this study, we sought to develop and apply our innovative RNAi NP platform to enable the first *in vivo* testing of a potent and selective therapy against mTORC2 in models of both *HER2*-amplified and triple-negative breast cancers.

Benefits of selective mTORC2 inhibition in *HER2*-amplified breast cancers

The PI3K/Akt/mTOR axis is often activated downstream of receptor tyrosine kinases (RTK) such as HER2, supporting the notion that RTK alterations would drive oncogenic mTORC2 signaling and Akt activation that drives tumor growth, progression, and treatment resistance. Abundant preclinical evidence suggests that Akt/mTOR inhibition is necessary for a full therapeutic response of *HER2*-amplified breast cancers (24, 46–48). Most studies have focused on inhibition of mTORC1, likely due to its position as a downstream effector of HER2/PI3K/Akt and the availability of mTORC1-specific inhibitors. Unfortunately, inhibition of mTORC1 relieves negative feedback on PI3K (through IRS-1), exacerbating RTK-dependent and -independent PI3K-to-Akt signaling, thus attenuating the realized therapeutic efficacy of mTORC1-specific rapalogs (8, 10). Considerably less is understood about the role of mTORC2 in breast cancer, but results from previous work demonstrate that mTORC2 inhibition (via RICTOR genetic ablation) results in apoptosis of HER2-amplified breast cancer cells, which could be circumvented by expression of constitutively active Akt mutants (24). These studies highlight the importance of mTORC2-Akt signaling in survival of breast cancer cells (24). In addition to Akt, mTORC2 activates other AGC kinases, including PKC isoforms and SGK isoforms, which contribute to cell proliferation and survival (16). Thus, while mTORC2 activation occurs as part of the linear RTK–PI3K–mTORC2–Akt–mTORC1 pathway, the effects of mTORC2 also impact other signaling pathways. Moreover, mTORC2 inhibition may have additional effects upon the tumor microenvironment that are currently understudied (49), raising the possibility that tumor growth inhibition in response to Rictor si-NPs is also due in part to yet unknown effects in the tumor microenvironment. On the basis of the role of mTORC2 in numerous signaling pathways within tumor cells, and potentially numerous cell types within tumors, it is logical that mTORC2 inhibition using Rictor si-NPs in combination with lapatinib decreased $HER2^{+}$ tumor growth to a greater extent than lapatinib alone (Fig. 5D–F). Although we show these two therapies cooperate to increase cell killing and reduce tumor growth, additional studies are needed to fully elucidate the molecular mechanisms that drive this effect.

A potential role for selective mTORC2 inhibition in TNBCs

Our analysis of publicly available breast cancer expression datasets revealed that *RICTOR* expression correlates with poor outcome in some, but not all, molecular subtypes of TNBC. Additional evidence that mTORC2 signaling might drive tumor progression in TNBCs has been previously shown. For example, *AKT1*, *AKT2*, and *AKT3* are often amplified or harbor activating mutations in TNBCs (50). In addition, mTORC2 is activated by the planar cell polarity (PCP) complex, a protein complex driving cell motility and metastasis in TNBCs (51), or by aberrant signaling of pRb, a protein frequently altered in TNBCs (52). Other groups have shown that SGK3, another mTORC2 substrate, is frequently hyperactivated in TNBCs (17). These data support the hypothesis that mTORC2 is potentially a high profile therapeutic molecular target in TNBCs. Indeed, our data show that genetic ablation of Rictor in TNBC cells and xenografts (MDA-MB-231) decreases cell survival and blocks tumor growth. While other groups have used Rictor RNAi to demonstrate decreased cell motility and cell survival in cultured MDA-MB-231 cells (27, 51), our RNAi approach is novel in that we have developed a translatable RNAi delivery platform that enables stable, efficient, and safe systemic delivery of RNAi sequences to tumors through intravenous injection *in vivo*, as described below.

Development of target-selective si-NPs for proteins that elude small-molecule inhibitors

Signaling complexes such as mTORC2 that form from many protein–protein interactions are notoriously difficult to drug by conventional pharmacology using small-molecule inhibitors. Clinical translation of intravenous-delivered siRNA for cancer treatment could circumvent the need for small-molecule drugs, but remains limited by systemic and intracellular pharmacokinetic barriers (53–61). We employed a recently published si-NP, optimized for improved resistance against heparin-induced disassembly in the kidneys, increased circulation time, enhanced pH-dependent endosomal escape for cytosol-specific delivery, and efficient gene silencing *in vitro* and *in vivo*. This delivery platform yielded superior gene silencing of the model gene luciferase compared with previous prototypes, but has yet to be assessed as a therapeutic for the ablation of cancer-causing genes within tumors (29). We show here that Rictor si-NPs that were generated using these recently developed technologies potently eliminated Rictor expression and blocked tumor growth in models of *HER2*-amplified and triple-negative breast cancer, highlighting for the first time both the feasibility of this approach and efficacy of an mTORC2-selective inhibitor. Interestingly, we found that systemic delivery of Rictor si-NPs in the acute setting of our studies had no effect on serum glucose levels (Supplementary Fig. S9), but further studies will be needed to fully appreciate the connection between systemic mTORC2-specific inhibition and gluconeogenesis due to the role of mTORC2/Akt signaling in the liver and kidneys.

Conclusion

In sum, this work introduces a selective mTORC2 inhibitor enabled by RNAi nanotechnology and validates its therapeutic utility in *HER2*-amplified and triple-negative breast cancers. Our results confirm that mTORC2 is a viable therapeutic target

in *HER2*-amplified breast cancers and provide mechanistic insight into response of *HER2*-amplified breast cancers to TKIs in combination with mTORC2-specific inhibition. Moreover, our mTORC2-specific inhibitor shows promise as a molecular targeted therapy for TNBC patients, who currently lack any options for targeted inhibitors. Our collective results motivate ongoing studies to catalog breast cancer subtype sensitivity to Rictor/mTORC2 RNAi, further elucidate relative importance of mTORC2 versus mTORC1 signaling, compare relevant on- and off-target toxicities of mTORC2 versus dual mTORC1/2 inhibition, and identify drug combinations with the greatest clinical potential.

Disclosure of Potential Conflicts of Interest

No potential conflicts of interest were disclosed.

Authors' Contributions

Conception and design: T.A. Werfel, D.M. Brantley-Sieders, R.S. Cook, C. Duvall

Development of methodology: T.A. Werfel, S. Wang, V. Sanchez, R.S. Cook

Acquisition of data (provided animals, acquired and managed patients, provided facilities, etc.): T.A. Werfel, M.A. Jackson, T.E. Kavanaugh, M.M. Joly, L. Lee, D.J. Hicks, V. Sanchez, K.V. Kilchrist, S.C. Dimobi, D.M. Brantley-Sieders, R.S. Cook

Analysis and interpretation of data (e.g., statistical analysis, biostatistics, computational analysis): T.A. Werfel, S. Wang, P.I. Gonzalez-Ericsson, K.V. Kilchrist, S.C. Dimobi, S.M. Sarett, D.M. Brantley-Sieders, C. Duvall

Writing, review, and/or revision of the manuscript: T.A. Werfel, S. Wang, M.A. Jackson, T.E. Kavanaugh, M.M. Joly, S.M. Sarett, D.M. Brantley-Sieders, R.S. Cook, C. Duvall

Administrative, technical, or material support (i.e., reporting or organizing data, constructing databases): S. Wang, D.J. Hicks

Study supervision: D.M. Brantley-Sieders, R.S. Cook, C. Duvall

Acknowledgments

We would like to acknowledge the shared resources at Vanderbilt University, Vanderbilt University Medical Center, and the Vanderbilt-Ingram Cancer Center that contributed to the studies reported herein, including the VICC Breast SPORE pathology service under the direction of Dr. Melinda Sanders, the VUMC Translational Pathology Shared Resource under the direction of Dr. Kelli Boyd, the Vanderbilt Digital Histology Shared Resource (DHSR) under the direction of Joseph Roland for access to a slide scanner and assistance with histology quantification, and the Vanderbilt Institute for Nanoscale Science and Engineering (VINSE) under the direction of Dr. Sandy Rosenthal for access to DLS and TEM (NSF EPS 1004083) instruments. This work was supported by Specialized Program of Research Excellence (SPORE) grant NIH P50 CA098131 (VICC; to R. S. Cook, D. J. Hicks, V. Sanchez, and P. Gonzalez Ericsson), Cancer Center Support grant NIH P30 CA68485 (VICC; to R.S. Cook, D. J. Hicks, V. Sanchez, and P. Gonzalez Ericsson), NIH R01 EB019409 (to T.A. Werfel, C.L. Duvall), DOD CDMRP OR130302 (to T. A. Werfel, T.E. Kavanaugh, C.L. Duvall), NSF GFRP 1445197 (to T.A. Werfel, M.A. Jackson, T.E. Kavanaugh, K.V. Kilchrist, S.M. Sarett), and CTSA UL1TR000445 (R. S. Cook) from the National Center for Advancing Translational Sciences.

The costs of publication of this article were defrayed in part by the payment of page charges. This article must therefore be hereby marked *advertisement* in accordance with 18 U.S.C. Section 1734 solely to indicate this fact.

Received August 10, 2017; revised October 11, 2017; accepted January 17, 2018; published OnlineFirst January 22, 2018.

References

1. Ross JS, Fletcher JA. The HER-2/neu oncogene in breast cancer: prognostic factor, predictive factor, and target for therapy. Stem Cells 1998;16:413–28.
2. Arteaga CL, Sliwkowski MX, Osborne CK, Perez EA, Puglisi F, Gianni L. Treatment of HER2-positive breast cancer: current status and future perspectives. Nat Rev Clin Oncol 2012;9:16–32.
3. Miller T, Rexer B, Garrett J, Arteaga C. Mutations in the phosphatidylinositol 3-kinase pathway: role in tumor progression and therapeutic implications in breast cancer. Breast Cancer Res 2011;13:224.
4. Miller TW, Balko JM, Arteaga CL. Phosphatidylinositol 3-Kinase and antiestrogen resistance in breast cancer. J Clin Oncol 2011;29:4452–61.
5. Laplante M, Sabatini David M. mTOR signaling in growth control and disease. Cell 2012;149:274–93.
6. Sarbassov DD, Ali SM, Sengupta S, Sheen J-H, Hsu PP, Bagley AF, et al. Prolonged rapamycin treatment inhibits mTORC2 assembly and Akt/PKB. Mol Cell 2006;22:159–68.
7. Palm W, Park Y, Wright K, Pavlova Natalya N, Tuveson David A, Thompson Craig B. The utilization of extracellular proteins as nutrients is suppressed by mTORC1. Cell 2015;162:259–70.
8. O'Reilly KE, Rojo F, She QB, Solit D, Mills GB, Smith D, et al. mTOR inhibition induces upstream receptor tyrosine kinase signaling and activates Akt. Cancer Res 2006;66:1500–8.
9. Rozengurt E, Soares HP, Sinnet-Smith J. Suppression of feedback loops mediated by PI3K/mTOR induces multiple overactivation of compensatory pathways: an unintended consequence leading to drug resistance. Mol Cancer Ther 2014;13:2477–88.
10. Carracedo A, Ma L, Teruya-Feldstein J, Rojo F, Salmena L, Alimonti A, et al. Inhibition of mTORC1 leads to MAPK pathway activation through a PI3K-dependent feedback loop in human cancer. J Clin Invest 2008;118.
11. Yuan HX, Guan KL. The SIN1-PH domain connects mTORC2 to PI3K. Cancer Discov 2015;5:1127–9.
12. Garcia-Martinez JM, Alessi DR. mTOR complex 2 (mTORC2) controls hydrophobic motif phosphorylation and activation of serum- and glucocorticoid-induced protein kinase 1 (SGK1). Biochem J 2008;416:375–85.
13. Guertin DA, Stevens DM, Thoreen CC, Burds AA, Kalaany NY, Moffat J, et al. Ablation in mice of the mTORC components raptor, rictor, or mLST8 reveals that mTORC2 is required for signaling to Akt-FOXO and PKCalpha, but not S6K1. Develop Cell 2006;11:859–71.
14. Kim LC, Cook RS, Chen J. mTORC1 and mTORC2 in cancer and the tumor microenvironment. Oncogene 2016;36:2191–201.
15. Morrison MM, Young CD, Wang S, Sobolik T, Sanchez VM, Hicks DJ, et al. mTOR directs breast morphogenesis through the PKC-alpha-Rac1 signaling axis. PLoS Genet 2015;11:e1005291.
16. Zoncu R, Efeyan A, Sabatini DM. mTOR: from growth signal integration to cancer, diabetes and ageing. Nat Rev Mol Cell Biol 2011;12:21–35.
17. Gasser Jessica A, Inuzuka H, Lau Alan W, Wei W, Beroukhim R, Toker A. SGK3 mediates INPP4B-dependent PI3K signaling in breast cancer. Mol Cell 2014;56:595–607.
18. Sommer EM, Dry H, Cross D, Guichard S, Davies BR, Alessi DR. Elevated SGK1 predicts resistance of breast cancer cells to Akt inhibitors. Biochem J 2013;452:499–508.
19. Hutchinson J, Jin J, Cardiff RD, Woodgett JR, Muller WJ. Activation of Akt (protein kinase B) in mammary epithelium provides a critical cell survival signal required for tumor progression. Mol Cell Biol 2001;21:2203–12.
20. Sarbassov DD, Guertin DA, Ali SM, Sabatini DM. Phosphorylation and regulation of Akt/PKB by the rictor-mTOR complex. Science 2005;307:1098–101.
21. Stiles B, Gilman V, Khanzenzon N, Lesche R, Li A, Qiao R, et al. Essential role of AKT-1/protein kinase B alpha in PTEN-controlled tumorigenesis. Mol Cell Biol 2002;22:3842–51.
22. Sun M, Wang G, Paciga JE, Feldman RI, Yuan ZQ, Ma XL, et al. AKT1/PKBalpha kinase is frequently elevated in human cancers and its constitutive activation is required for oncogenic transformation in NIH3T3 cells. Am J Pathol 2001;159:431–7.
23. Hatakeyama J, Wald JH, Printsev I, Ho HY, Carraway KL III. Vangl1 and Vangl2: planar cell polarity components with a developing role in cancer. Endocr Relat Cancer 2014;21:R345–56.

24. Morrison-Joly M, Hicks DJ, Jones B, Sanchez V, Estrada MV, Young C, et al. Rictor/mTORC2 drives progression and therapeutic resistance of HER2-amplified breast cancers. Cancer Res 2016;76:4752–64.
25. Morrison Joly M, Williams MM, Hicks DJ, Jones B, Sanchez V, Young CD, et al. Two distinct mTORC2-dependent pathways converge on Rac1 to drive breast cancer metastasis. Breast Cancer Res 2017;19:74.
26. Zhang F, Zhang X, Li M, Chen P, Zhang B, Guo H, et al. mTOR complex component Rictor interacts with PKCzeta and regulates cancer cell metastasis. Cancer Res 2010;70:9360–70.
27. Li H, Lin J, Wang X, Yao G, Wang L, Zheng H, et al. Targeting of mTORC2 prevents cell migration and promotes apoptosis in breast cancer. Breast Cancer Res Treat 2012;134:1057–66.
28. Hietakangas V, Cohen SM. TOR complex 2 is needed for cell cycle progression and anchorage-independent growth of MCF7 and PC3 tumor cells. BMC Cancer 2008;8:282.
29. Werfel T, Jackson M, Kavanaugh T, Kirkbride K, Miteva M, Giorgio T, et al. Combinatorial optimization of PEG architecture and hydrophobic content improves siRNA polyplex stability, pharmacokinetics, and potency in vivo. J Control Release 2017;255:12–26.
30. Young L, Sung J, Stacey G, Masters JR. Detection of Mycoplasma in cell cultures. Nat Protoc 2010;5:929.
31. Nelson CE, Kintzing JR, Hanna A, Shannon JM, Gupta MK, Duvall CL. Balancing cationic and hydrophobic content of PEGylated siRNA polyplexes enhances endosome escape, stability, blood circulation time, and bioactivity in vivo. ACS Nano 2013;7:8870–80.
32. Kilchrist KV, Evans BC, Brophy CM, Duvall CL. Mechanism of enhanced cellular uptake and cytosolic retention of MK2 inhibitory peptide nanopolyplexes. Cell Mol Bioeng 2016;9:368–81.
33. Morrison MM, Hutchinson K, Williams MM, Stanford JC, Balko JM, Young C, et al. ErbB3 downregulation enhances luminal breast tumor response to antiestrogens. J Clin Invest 2013;123:4329–43.
34. Bergers G, Brekken R, McMahon G, Vu TH, Itoh T, Tamaki K, et al. Matrix metalloproteinase-9 triggers the angiogenic switch during carcinogenesis. Nat Cell Biol 2000;2:737–44.
35. Qu S, Rinehart C, Wu HH, Wang SE, Carter B, Xin H, et al. Gene targeting of ErbB3 using a Cre-mediated unidirectional DNA inversion strategy. Genesis 2006;44:477–86.
36. Youngblood V, Wang S, Song W, Walter D, Hwang Y, Chen J, et al. Elevated slit2 activity impairs VEGF-induced angiogenesis and tumor neovascularization in EphA2-deficient endothelium. Mol Cancer Res 2015;13:524–37.
37. Evans BC, Nelson CE, Yu SS, Beavers KR, Kim AJ, Li H, et al. Ex vivo red blood cell hemolysis assay for the evaluation of pH-responsive endosomolytic agents for cytosolic delivery of biomacromolecular drugs. J Vis Exp 2013;73:e50166.
38. Wittrup A, Ai A, Liu X, Hamar P, Trifonova R, Charisse K, et al. Visualizing lipid-formulated siRNA release from endosomes and target gene knockdown. Nat Biotech 2015;33:870–6.
39. Lehmann BD, Bauer JA, Chen X, Sanders ME, Chakravarthy AB, Shyr Y, et al. Identification of human triple-negative breast cancer subtypes and preclinical models for selection of targeted therapies. J Clin Invest 2011;121:2750–67.
40. Zuckerman JE, Choi CH, Han H, Davis ME. Polycation-siRNA nanoparticles can disassemble at the kidney glomerular basement membrane. Proc Natl Acad Sci U S A 2012;109:3137–42.
41. Wander SA, Hennessy BT, Slingerland JM. Next-generation mTOR inhibitors in clinical oncology: how pathway complexity informs therapeutic strategy. J Clin Invest 2011;121:1231–41.
42. Janku F, Tsimberidou AM, Garrido-Laguna I, Wang X, Luthra R, Hong DS, et al. PIK3CA mutations in patients with advanced cancers treated with PI3K/AKT/mTOR axis inhibitors. Mol Cancer Ther 2011;10:558–65.
43. Janku F, Wheler JJ, Westin SN, Moulder SL, Naing A, Tsimberidou AM, et al. PI3K/AKT/mTOR inhibitors in patients with breast and gynecologic malignancies harboring PIK3CA mutations. J Clin Oncol 2012;30:777–82.
44. Janku F, Wheler JJ, Naing A, Falchook GS, Hong DS, Stepanek VM, et al. PIK3CA mutation H1047R is associated with response to PI3K/AKT/mTOR signaling pathway inhibitors in early-phase clinical trials. Cancer Res 2013;73:276–84.
45. Garcia-Garcia C, Ibrahim YH, Serra V, Calvo MT, Guzman M, Grueso J, et al. Dual mTORC1/2 and HER2 blockade results in antitumor activity in preclinical models of breast cancer resistant to anti-HER2 therapy. Clin Cancer Res 2012;18:2603–12.
46. Miller TW, Forbes JT, Shah C, Wyatt SK, Manning HC, Olivares MG, et al. Inhibition of mammalian target of rapamycin is required for optimal antitumor effect of HER2 inhibitors against HER2-overexpressing cancer cells. Clin Cancer Res 2009;15:7266–76.
47. Engelman JA. Targeting PI3K signalling in cancer: opportunities, challenges and limitations. Nat Rev Cancer 2009;9:550–62.
48. Nahta R, O'Regan RM. Evolving strategies for overcoming resistance to HER2-Directed therapy: targeting the PI3K/Akt/mTOR pathway. Clin Breast Cancer 2010;10:S72–S8.
49. Kim LC, Cook RS, Chen J. mTORC1 and mTORC2 in cancer and the tumor microenvironment. Oncogene 2016;36:2191.
50. Balko JM, Cook RS, Vaught DB, Kuba MG, Miller TW, Bhola NE, et al. Profiling of residual breast cancers after neoadjuvant chemotherapy identifies DUSP4 deficiency as a mechanism of drug resistance. Nat Med 2012;18:1052–9.
51. Daulat AM, Bertucci F, Audebert S, Serge A, Finetti P, Josselin E, et al. PRICKLE1 contributes to cancer cell dissemination through its interaction with mTORC2. Dev Cell 2016;37:311–25.
52. Zhang J, Xu K, Liu P, Geng Y, Wang B, Gan W, et al. Inhibition of Rb phosphorylation leads to mTORC2-mediated activation of Akt. Mol Cell 2016;62:929–42.
53. Nakayama T, Butler JS, Sehgal A, Severgnini M, Racie T, Sharman J, et al. Harnessing a physiologic mechanism for siRNA delivery with mimetic lipoprotein particles. Mol Thera 2012;20:1582–9.
54. Rajeev KG, Nair JK, Jayaraman M, Charisse K, Taneja N, O'Shea J, et al. Hepatocyte-specific delivery of siRNAs conjugated to novel non-nucleosidic trivalent N-acetylgalactosamine elicits robust gene silencing in vivo. Chembiochem 2015;16:903–8.
55. Yasuda M, Gan L, Chen B, Kadirvel S, Yu C, Phillips JD, et al. RNAi-mediated silencing of hepatic Alas1 effectively prevents and treats the induced acute attacks in acute intermittent porphyria mice. Proc Nat Acad Sci U S A 2014;111:7777–82.
56. Coelho T, Adams D, Silva A, Lozeron P, Hawkins PN, Mant T, et al. Safety and efficacy of RNAi therapy for transthyretin amyloidosis. N Engl J Med 2013;369:819–29.
57. Matsuda S, Keiser K, Nair JK, Charisse K, Manoharan RM, Kretschmer P, et al. siRNA conjugates carrying sequentially assembled trivalent N-acetylgalactosamine linked through nucleosides elicit robust gene silencing in vivo in hepatocytes. ACS Chem Biol 2015;10:1181–7.
58. Frank-Kamenetsky M, Grefhorst A, Anderson NN, Racie TS, Bramlage B, Akinc A, et al. Therapeutic RNAi targeting PCSK9 acutely lowers plasma cholesterol in rodents and LDL cholesterol in nonhuman primates. Proc Nat Acad Sci U S A 2008;105:11915–20.
59. Wang J, Lu Z, Wientjes MG, Au JL. Delivery of siRNA therapeutics: barriers and carriers. AAPS J 2010;12:492–503.
60. Gilleron J, Querbes W, Zeigerer A, Borodovsky A, Marsico G, Schubert U, et al. Image-based analysis of lipid nanoparticle-mediated siRNA delivery, intracellular trafficking and endosomal escape. Nat Biotechnol 2013;31:638–46.
61. Haussecker D. Current issues of RNAi therapeutics delivery and development. J Control Release 2014;195:49–54.